Atmos. Chem. Phys. Discuss., 15, 21671–21711, 2015
www.atmos-chem-phys-discuss.net/15/21671/2015/
doi:10.5194/acpd-15-21671-2015

Atmospheric Chemistry and Physics Discussions

Understanding cirrus ice crystal number variability for different heterogeneous ice nucleation spectra

S. C. Sullivan[1], R. Morales Betancourt[2,a], D. Barahona[3], and A. Nenes[1,2,4]

[1]Department of Chemical and Biomolecular Engineering, Georgia Institute of Technology, Atlanta, GA 30332, USA
[2]Department of Earth and Atmospheric Sciences, Georgia Institute of Technology, Atlanta, GA 30332, USA
[3]NASA Goddard Space Flight Center, Greenbelt, MD 20771, USA
[4]ICE-HT, Foundation for Research and Technology, Hellas, 26504 Patras, Greece
[a]now at: Department of Civil Engineering, University of Los Andes, Bogotá, Colombia

Received: 16 June 2015 – Accepted: 18 June 2015 – Published: 11 August 2015

Correspondence to: A. Nenes (athanasios.nenes@gatech.edu)

Published by Copernicus Publications on behalf of the European Geosciences Union.

Abstract

Along with minimizing parameter uncertainty, understanding the cause of temporal and spatial variability of nucleated ice crystal number, N_i, is key to improving the representation of cirrus clouds in climate models. To this end, sensitivities of N_i to input variables like aerosol number and diameter provide valuable information about nucleation regime and efficiency for a given model formulation. Here we use the adjoint model of the Barahona and Nenes cirrus formation parameterization to understand N_i variability for various ice-nucleating particle (INP) spectra. Inputs are generated with the Community Atmosphere Model version 5, and simulations are done with a theoretically-derived spectrum, a lab-based empirical spectrum, and two field-based empirical spectra that differ in the nucleation threshold for black carbon aerosol and in the active site density for dust. The magnitude and sign of N_i sensitivity to insoluble aerosol number can be directly linked to nucleation regime and efficiency of various INP. The lab-based spectrum calculates much higher INP efficiencies than field-based ones, which reveals a disparity in aerosol surface properties. N_i sensitivity to temperature tends to be low, due to the compensating effects of temperature on INP spectrum parameters; this low temperature sensitivity regime has been experimentally reported before but never unraveled as done here.

1 Introduction

Aerosol–cloud interactions remain the largest source of uncertainty in projections of anthropogenic climate change, and aerosol–ice interactions, in particular, are poorly understood (Boucher et al., 2013). Atmospheric aerosol may modulate the properties of pure ice clouds by providing particles upon which new ice crystals form. Cirrus clouds control moisture transfer into the lower stratosphere and can have a net warming effect (Gettelman et al., 2002).

ACPD
15, 21671–21711, 2015

Ice crystals within cirrus clouds can be formed in a variety of ways. Heterogeneous nucleation refers to the formation of ice on an aerosol surface, and the portion of aerosol upon which ice forms this way are called ice-nucleating particles (INP). There are several modes of heterogeneous freezing: in deposition nucleation, vapor deposits directly onto an aerosol; in condensation freezing, the aerosol acts first as a cloud condensation nucleus and then immediately as an INP; and in immersion freezing, an aerosol submerged for some time in supercooled liquid eventually initiates ice formation. Ice crystals may also form directly from an aqueous phase through homogeneous nucleation, typically at temperatures below about 235 K (Pruppacher and Klett, 1997). Both mechanisms can be active in cirrus clouds, and the competition for water vapor between homogeneous and heterogeneous ice formation must be treated in cirrus formation parameterizations (Barahona and Nenes, 2008, 2009a, b; Lin et al., 2005).

Much effort has been devoted to studying heterogeneous ice nucleation on a fundamental level (e.g., Reinhardt and Doye, 2014; Lupi et al., 2014; Cox et al., 2015). Heterogenous nucleation can be understood as the formation of an ice germ in the vicinity of an active site. The nature of active sites is unknown, but current understanding suggests that they promote ordering of the water molecule layers near the particle surface. The active site density refers to the number of these sites per unit of aerosol surface area. A particle with more surface area will tend to have more active sites and nucleate at higher temperatures (or lower supersaturations); however, each active site varies in its efficiency, so that contact angle or site density distributions are necessary (Barahona, 2012; Kulkarni et al., 2012).

While Köhler theory is the accepted framework to describe droplet activation, nothing analogous exists for ice. Two conceptual paradigms are currently in use: stochastic and singular freezing (Pruppacher and Klett, 1997; Vali, 2014). In the stochastic paradigm, water molecules fluctuate randomly to and from a particle surface with some probability of reaching a critical, stable germ size that initiates formation of the new phase; homogeneous nucleation within a supercooled droplet can be understood this way. In the singular paradigm, nucleation is determined solely by particle surface morphology;

ACPD
15, 21671–21711, 2015

once a characteristic threshold temperature or supersaturation is acquired, ice nucleates.

Parameterizations of heterogeneous ice nucleation calculate the heterogeneously-formed ice crystal number, $N_{i,\,het}$, as a function of thermodynamic conditions and precursor aerosol properties. These parameterizations, termed INP spectra hereafter, may be empirically or theoretically based. Empirical spectra use lab or field data to calculate an active site density. Theoretically based spectra use classical nucleation theory and calculate a nucleation rate proportional to the aerosol surface area (e.g., Kärcher and Lohmann, 2002; Liu and Penner, 2005; Niemand et al., 2012; Barahona and Nenes, 2009b; Marcolli et al., 2007). The surface heterogeneity should also be considered and has recently been represented as a distribution of contact angles (Savre et al., 2013; Wang et al., 2014). But ice nucleation data is geographically- or thermodynamically-limited, taken only in localized regions or over a narrow range of temperatures and pressures. And classical nucleation theory is approximate and requires unknown or variable surface property data. As a result, the output of INP spectra has remained uncertain, with up to three orders of magnitude difference in calculated N_i (e.g., Barahona et al., 2010).

Early published INP spectra expressed active site density as a function of only temperature or supersaturation and neglected the aerosol composition and size. For example, Fletcher 1969 proposed a parameterization based solely on temperature, valid down to about −25 °C. The Meyers et al. INP spectrum describes deposition and condensation nucleation as a function of supersaturation only, with data from a continuous-flow diffusion chamber (Meyers et al., 1992). They observed a logarithmic increase in the number of ice-nucleating aerosol with supersaturation with respect to ice, S_i.

More recently published INP spectra consider the effects of size distribution and composition of ice-nucleating particles. For example, Phillips et al. (2008) (PDA08) calculates the active site density for mineral dust, black carbon, and hydrophobic organics, constrained with data from the First and Second Ice Nuclei Spectroscopy campaigns (INSPECT-1 and -2) and the Cirrus Regional Study of Tropical Anvils and Cirrus Lay-

ACPD
15, 21671–21711, 2015

ers – Florida-Area Cirrus Experiment (CRYSTAL-FACE) (Phillips et al., 2008). Updates have been made in the Phillips et al. (2013) spectrum (PDA13). PDA08 and PDA13 are based on the singular paradigm, in which each aerosol type nucleates ice at threshold temperatures and supersaturations. Several other studies have parameterized nucleation efficiency of mineral dusts or illite powders, using cloud chamber data or optical microscopy (e.g., Connolly et al., 2009; Niedermeier et al., 2010; Broadley et al., 2012; Niemand et al., 2012). Hiranuma et al. have also developed an INP spectrum at cirrus-relevant temperatures, using the Aerosol Interaction and Dynamics in the Atmosphere (AIDA) cloud chamber data for hematite particles (Hiranuma et al., 2014). This study uses the three aforementioned spectra. Other empirical spectra and recent heterogeneous ice nucleation experiments are further discussed in the review by Hoose and Möhler (2012).

Numerous studies have examined the impact of INP spectrum on nucleated ice crystal number. Using the NCAR Community Atmosphere Model (CAM), Xie et al. evaluated how predicted cloud type, cloud properties, and radiative balance change with the INP spectrum (Xie et al., 2013). The study uses Meyers et al. (1992) as a default spectrum compared to DeMott et al. (2010), a spectrum which links N_i with the aerosol number of diameter larger than 0.5 µm. DeMott et al. calculated a much lower N_i, and hence a higher liquid water path and lower ice water path for Arctic mixed-phase clouds. Curry and Khvorostyanov have also run Meyers et al. (1992), DeMott et al. (1998), Phillips et al. (2008), and their own theoretical INP spectra with parcel model simulations over a range of thermodynamic conditions (Curry and Khvorostyanov, 2012). The authors emphasize the importance of applying empirical spectra only in their regions of validity and note that low nucleating efficiencies in PDA08 may underestimate ice crystal number. Prenni et al. noted that Meyers et al. significantly overpredicted ice water content in coupled models if aerosol were not depleted after nucleation (Prenni et al., 2007). When INP depletion was included, the predictions of water and ice in mixed-phase clouds improved considerably. Barahona et al. compared the output crystal number between PDA08, Meyers et al. (1992), Murray et al. (2010), and the

ACPD
15, 21671–21711, 2015

Barahona and Nenes CNT spectrum for both monodisperse and polydisperse aerosol (Barahona et al., 2010). They found that ice nucleation occurred more often in the competitive regime for the Meyers et al. spectrum, yielding smaller crystal numbers; however, PDA08 predicted higher crystal numbers with ice nucleation most frequently in the homogeneous regime. Similar results have also been reported for mixed-phase cloud conditions (e.g., Morales-Betancourt et al., 2012).

In this work, we extend the adjoint of a cirrus formation parameterization (Sheyko et al., 2015) to perform sensitivity analysis for several heterogeneous INP spectra. Adjoints can calculate the sensitivity of a given output to all inputs more efficiently and accurately than finite difference runs, but at the expense of code development (Errico, 1997; Giering and Kaminski, 1998). Karydis et al. have constructed the adjoint model of a liquid droplet parameterization, and others have used adjoints for data assimilation, for example in the Community Multiscale Air Quality and ISORROPIA models (Hakami et al., 2007; Karydis et al., 2012; Capps et al., 2012). Here we use the adjoint approach to address the following: how and why N_i and its sensitivities change with the INP spectrum used and how sensitivities can elucidate nucleation regime and efficiency. Our focus is on spatial and temporal output variability, distinct from output uncertainty. The development of heterogeneous ice nucleation spectra reduces parameter uncertainty; once a spectrum is chosen, the question of how input variables contribute to output variability remains. We consider the latter here. Section 2 provides an overview of the nucleation parameterization, model inputs, and four INP spectra used. Crystal number fields and aerosol acting as INP are presented in Sects. 3.1 and 3.2. Sensitivities of different spectra are discussed in Sects. 3.3 to 3.6, and Sect. 4 summarizes the work.

ACPD
15, 21671–21711, 2015

2 Methods

2.1 BN parameterization

We use the Barahona and Nenes cirrus formation parameterization (BN09) (Barahona and Nenes, 2008, 2009a, b) and its adjoint (Sheyko et al., 2015). BN09 describes the competition for water vapor between heterogeneous and homogeneous nucleation; the number of heterogeneously-formed crystals, $N_{\mathrm{i,\,het}}$, is calculated from any of a variety of nucleation spectra, and homogeneously-formed number, $N_{\mathrm{i,\,hom}}$, is calculated with an approximate solution to the coupled mass and energy balances of a cirrus cloud parcel. Then the total ice crystal number, N_{i}, is the sum of the heterogeneous and homogeneous contributions (Eq. 1). When the temperature is greater than about −38 °C, homogeneous nucleation ceases because it is kinetically unfavorable. Homogeneous nucleation is also suppressed when the number of INP exceeds a certain threshold, N_{lim}, and the maximum supersaturation that develops within the cloud parcel, s_{max}, is less than the threshold for homogeneous nucleation, s_{hom}. In this case, s_{max} must be numerically calculated from the growth and supersaturation evolution equations.

$$N_{\mathrm{i}} = \begin{cases} N_{\mathrm{i,\,hom}} + N_{\mathrm{i,\,het}}(s_{\mathrm{hom}}), N_{\mathrm{i,\,het}}(s_{\mathrm{hom}}) < N_{\mathrm{lim}} \\ N_{\mathrm{i,\,het}}(s_{\mathrm{max}}), N_{\mathrm{i,\,het}}(s_{\mathrm{hom}}) \geq N_{\mathrm{lim}} \end{cases} \quad (1)$$

As in Sheyko et al., the TAPENADE automatic differentiation tool was used to create an adjoint model of BN09 (ABN15 hereafter) (Hascoët and Pascual, 2004). For the finite series of operations that link N_{i} to the inputs in BN09, TAPENADE uses the chain rule to propagate a perturbation in the output, $\mathrm{d}N_{\mathrm{i}}$, back to differentials in the input variables. Once developed, the adjoint model saves significant computational time, relative to a finite difference method, and avoids both approximation and truncation errors. ABN15 differentiates N_{i} with respect to 13 input variables: temperature; updraft velocity; accumulation and coarse mode dust numbers and diameters; organic aerosol number and diameter; black carbon number and diameter; sulfate number and diameter; and

ACPD
15, 21671–21711, 2015

water vapor deposition coefficient. All derivatives, along with the typical output of BN09, are evaluated at the input model state for each grid cell and time step of a GCM run. ABN15 is verified with centered finite difference approximations, using perturbations of ±0.1 % around each input for simulation-relevant thermodynamic and aerosol conditions. Such finite difference calculations require two runs for each variable, so for 13 input variables, the adjoint model saves 25 executions of the parameterization relative to typical sensitivity calculations.

2.2 Simulation setup and spectra

Simulation inputs are generated from the NCAR Community Atmosphere Model, version 5 (CAM5) at the 232 hPa pressure level with two year spin-up and 2.5° × 1.88° resolution. The altitude examined is in the middle of the ISCCP cloud classification for cirrus (pressures between 440 and 50 hPa) and represents pure ice cloud formation. The Lamarque et al. emissions inventory (Lamarque et al., 2010) and MAM3 module were used (Liu et al., 2012a). Lognormal size distributions are assumed for all aerosol types with geometric standard deviations, σ_g, assumed constant and listed below in Table 1. σ_g and total aerosol mass are used to determine geometric mean diameter for each mode. Total aerosol number is scaled by mass fraction to determine aerosol number concentrations in each mode (Morales-Betancourt and Nenes, 2014). For calculations of ice crystal number concentrations and sensitivities, BN09 and ABN15 were run over a year with four heterogeneous INP spectra and daily-averaged values of CAM output.

2.3 Phillips et al. empirical spectra

PDA08 uses the exponential correlation of crystal number and supersaturation in Meyers et al. as a reference spectrum, extending the applicable ranges of temperature and supersaturation and incorporating characteristics of the precursor aerosol. The number of ice-nucleating particles, $N_{INP,X}$ in aerosol group X (dust and metallics – DM, black

ACPD
15, 21671–21711, 2015

carbon – BC, or organics – O) is calculated with a sum over the aerosol size distribution weighted by a freezing fraction:

$$N_{\mathrm{INP},X} = \int_{\log 0.1\,\mu\mathrm{m}}^{\infty} \{1 - \exp[-\mu_X(D, S_\mathrm{i}, T)]\}\; n_X(\log D)\; \mathrm{d}\log D \tag{2}$$

μ_X represents the number of ice embryos forming per aerosol and is the product of the active site density and aerosol surface area (Steinke et al., 2015): $\mu_X = H_X(S_\mathrm{i}, T)\xi(T)\left(\frac{\alpha_X\, N_{\mathrm{INP},*}}{\Omega_{X,*}}\right)\pi D^2$. H_X is a threshold function that reduces INP concentrations at conditions subsaturated with respect to water and warm sub-zero temperatures in agreement with observations; $\xi(T)$ suppresses heterogeneous nucleation at warm sub-zero temperatures; $N_{\mathrm{INP},*}$ is the INP number from a reference activity spectrum; $\Omega_{X,*}$ is a reference aerosol surface area, which acts as a normalization factor for the size distribution; α_X is the portion of aerosol number belonging to group X within $N_{\mathrm{INP},*}$; and $n_X(\log D)$ is the aerosol size distribution. H_X equals unity at water saturation and steps at certain threshold temperatures, $T_{0,X}$, and supersaturations, $s_{i,0,X}$, for the different aerosol groups. Finally $\xi(T)$ diminishes heterogeneous nucleation at warm sub-zero temperatures.

Both PDA08 and PDA13 adopt the mathematical framework of Eq. (2), but PDA13 employs more extensive field campaign data (Phillips et al., 2013). The organic classification in PDA13 is also split into primary biological material and glassy organics, following recent observations of distinct ice-nucleating activity for these particle types. In this study, sensitivity of N_i to biological INP is not considered, as CAM5 does not currently output a biological particle number.

ACPD
15, 21671–21711, 2015

2.4 Classical nucleation theory spectrum

We also use the classical nucleation spectrum developed by Barahona and Nenes and presented in conjunction with the parameterization (Barahona and Nenes, 2009b):

$$N_{\mathrm{INP},X} = e_X n_X(\log D)\min\left[\frac{S_\mathrm{i}}{S_{\mathrm{i},0,X}} e^{-f(\cos\theta)\ k_\mathrm{hom}\ (S_{\mathrm{i},0,X}-S_\mathrm{i})}, 1\right] \quad (3)$$

where e_X is the nucleation efficiency of aerosol group X, $S_{\mathrm{i},0,X}$ is the threshold supersaturation, $n_X(\log D)$ is the aerosol size distribution, θ is the INP-ice contact angle, and k_hom is a parameter related to the homogeneous nucleation threshold. Dust and black carbon groups are included with parameters listed in Table 1. The stochastic component of the nucleation efficiency through heterogeneous nucleation rate coefficient is assumed negligible, and the singular paradigm also underlies this spectrum. e_X is a function of temperature and the aerosol profile, but here its value is taken from the literature and assumed constant throughout the simulation.

2.5 Hiranuma et al. spectrum

The nucleation efficiency of hematite particles was measured at the AIDA chamber from −78 up to −36 °C and parameterized (Hiranuma et al., 2014). The third-order polynomial fit for active site density (in m^{-2}) is given in Eq. (4) as a function of temperature and ice saturation ratio. Isolines from AIDA expansion cooling experiments are interpolated over the temperature-supersaturation space, assuming a hematite baseline surface area of $6.3\times10^{-10}\ \mathrm{m}^2\ \mathrm{L}^{-1}$.

$$\begin{aligned} n_s(T,S_\mathrm{i}) = &-3.777\times10^{13} - 7.818\times10^{11}T + 4.252\times10^{13}S_\mathrm{i} - 4.598\times10^{9}T^2 \\ &+ 6.952\times10^{11}T\cdot S_\mathrm{i} - 1.111\times10^{13}S_\mathrm{i}^2 - 2.966\times10^{6}T^3 + 2.135\times10^{9}T^2\cdot S_\mathrm{i} \\ &- 1.729\times10^{11}T\cdot S_\mathrm{i}^2 - 9.438\times10^{11}S_\mathrm{i}^3 \end{aligned} \quad (4)$$

ACPD
15, 21671–21711, 2015

As in Hiranuma et al. (2014), we use this active site parameterization in the framework of Eq. (2) to calculate nucleated crystal number:

$$N_{\mathrm{INP},X} = \int_{\log 0.1\,\mu\mathrm{m}}^{\infty} \left\{1 - \exp\left[-n_s(T, S_\mathrm{i})\pi D^2\right]\right\} n_X(\log D)\, \mathrm{d}\log D. \quad (5)$$

Hereafter, we refer to this formulation as the AIDA spectrum.

3 Results

Homogeneous and heterogeneous nucleation can be active in cirrus clouds, and their relative influence can be conceptually understood along an INP-N_i trace shown in Fig. 1a (Ren and MacKenzie, 2005; Barahona and Nenes, 2009a). When INP concentration is low, nucleation is predominantly homogeneous. The slope or sensitivity here, $\partial N_\mathrm{i}/\partial N_\mathrm{INP}$, is slightly negative because the addition of an insoluble particle slightly decreases the number of nucleated ice crystals by competing for water vapor and decreasing supersaturation. As the INP concentration increases, homogeneous and heterogeneous nucleation compete more strongly for water vapor. Water vapor preferentially deposits on the additional INP surface and depresses the number of newly-nucleated crystals, so $\partial N_\mathrm{i}/\partial N_\mathrm{INP}$ increases in magnitude. Eventually, INP concentration increases beyond the threshold number, N_lim, and further depletion of supersaturation inhibits homogeneous nucleation altogether. Addition of another INP increases the ice crystal number, and $\partial N_\mathrm{i}/\partial N_\mathrm{INP}$ becomes positive. While all nucleation for $N_\mathrm{INP} < N_\mathrm{lim}$ is competitive, we use the term "competitive nucleation" below to refer to the case when both homogeneous and heterogeneous nucleation have a significant contribution, greater than 10 %, to N_i. These three regimes have been explained in terms of INP number, but they can also be understood in terms of INP diameter: in-

ACPD
15, 21671–21711, 2015

creasing INP surface area leads to more vapor depletion by heterogeneous nucleation and decreased crystal number in the competitive regime. This conceptual framework is used to understand the simulation results.

3.1 Crystal number

Figure 2e shows a comparison of in-situ ice crystal number measurements, compiled from a number of campaigns with large geographic coverage (Krämer et al., 2009) and annually-averaged N_i values versus input temperature. The parameterization calculates nucleated crystal number which tends to be higher than the in-cloud crystal number because the presence of preexisting ice crystals can inhibit ice nucleation (Barahona and Nenes, 2011). Sedimentation and autoconversion processes may also reduce N_i, and temperatures are too cold for secondary ice formation. Modeled N_i is still of the appropriate order, falling within the first and third quartiles of the data with the exception of a narrow temperature range around 205 K. Unexpectedly low N_i at the coldest temperatures and a corresponding model overestimate have been noted often (e.g., Barahona and Nenes, 2011; Spichtinger and Krämer, 2013). The modeled crystal number varies least for temperatures below 215 K, as homogeneous nucleation dominates and N_i becomes insensitive to INP spectrum. Above 215 K, the range broadens both within and between the spectra as heterogeneous nucleation affects N_i and the formulations diverge.

Figure 2a through d shows the annually-averaged potential nucleated ice crystal number for each grid cell, given the vertical velocity and aerosol profile. Some common features are observed: over the Himalayas and Rockies, N_i is higher because orographic lifting generates stronger updrafts and more supersaturation; the Saharan and Gobi desert outflows enhance $N_{i,\,het}$; and for INP spectra considering black carbon (all except the AIDA spectrum), higher $N_{i,\,het}$ occurs in regions of biomass burning (e.g., sub-Saharan Africa and the Amazon). In the Southern Hemisphere, especially over Antarctica, heterogeneous nucleation is rare and N_i stays high because aerosol number concentrations are low and active site density decreases with temperature.

ACPD
15, 21671–21711, 2015

Elsewhere, N_i is highly variable and sensitive to the INP spectrum. For example, all spectra except PDA08 see higher crystal number in the Northern than the Southern Hemisphere. In agreement with previous studies, PDA08 predicts the lowest INP number, between 0.047 and 5.07 L^{-1}, (Table 2) and the highest maximum supersaturations (Barahona et al., 2010; Curry and Khvorostyanov, 2012; Morales-Betancourt et al., 2012). When the input aerosol number is sufficiently high in the Northern Hemisphere, stronger competitive nucleation results in lower N_i, while the Southern Hemisphere remains dominated by homogeneous nucleation and higher N_i. Updraft velocity and N_i are well-correlated; both have higher values around the equator for PDA08.

Compared to PDA08, PDA13 predicts about an order of magnitude higher INP number, between 0.57 and 28.6 L^{-1} and more frequent inhibition of homogeneous nucleation. In localized regions of purely heterogeneous nucleation, however, PDA08 may still predict higher N_i. This can be understood in terms of an INP abundance, $A_{INP} \equiv N_{INP}/N_{lim}$, defined as the ratio of available INP to the limiting number to inhibit homogeneous nucleation. N_{lim} increases with decreasing maximum supersaturation, $N_{lim} \propto S_{i,\,max}/(S_{i,\,max} - 1)$, and this increase in N_{lim} can outweigh the increase in INP number so that A_{INP} actually decreases.

Whenever calculated supersaturations are similar between PDA08 and PDA13, higher N_i in PDA08 can also be understood in terms of threshold supersaturations for nucleation. When these thresholds are less stringent, the competitive nucleation cusp of the INP-N_i trace becomes steeper and extends to lower N_i values. Where nucleation is competitive, then, as in PDA13 around the equator, very low N_i is possible.

Compared to PDA13, INP numbers in the CNT and AIDA spectra are about tenfold higher, with median values of 50.38 and 52.51 L^{-1} respectively. These high INP numbers result in almost purely heterogeneous nucleation in the Northern Hemisphere and competitive nucleation in the Southern Hemisphere. INP increases lead to frequent inhibition of homogeneous ice nucleation. The highest crystal numbers in any of the fields occur for the CNT spectrum in Saharan outflows because of the high dust nucleation efficiency and the dependence on aerosol number concentration rather than

ACPD
15, 21671–21711, 2015

surface area here. Large accumulation mode dust numbers can yield large A_{INP}. N_i is on the order of $1\,L^{-1}$ here, larger than any of the in-situ measurements shown in Fig. 2. An overestimate of INP by CNT-based spectra has been reported elsewhere (e.g., Liu et al., 2012b). Again, higher N_i are due to higher A_{INP}: for these spectra, the increase in N_{lim} with decreasing supersaturation is not enough to outweigh the higher INP numbers.

Both PDA13 and AIDA spectra have a region of especially high N_i, south of a strong temperature gradient around 40° S. Even further south below another temperature gradient around 65° S, N_i drops off again over Antarctica. At the coldest temperatures, the threshold supersaturation for homogeneous nucleation significantly increases (Fig. 1b). When more INP are available, the system may be driven into the competitive nucleation regime. This transition is likely for the AIDA spectra, and even more so for PDA13, where the active site density parameterizations have a strong supersaturation dependence at low temperatures. Indeed, the active fraction of dust aerosol increases more within PDA13 than within AIDA in this region. Additionally, glassy organic aerosol activates at the coldest temperatures for PDA13 and exhibits a seasonal dependence (Fig. S1 in the Supplement).

3.2 Nucleating aerosol

We consider next which aerosol groups act as INP in the regions of purely heterogeneous nucleation. For PDA08 in Fig. 3a and c, both dust and black carbon play a role. Gradients in input temperature and BC contribution both appear around 40° S because the BC threshold supersaturation is a quadratic function of temperature in this spectrum (Fig. 1b) (Zuberi et al., 2002). Below 60° S, the BC contribution is 40 % or higher for PDA08, which is unexpected given the smaller land coverage and lower population density of the Southern Hemisphere.

For PDA13, dust is by far the primary contributor to $N_{i,\,het}$ outside of a very localized region of deep convection around the Equator. The correlation for $S_{i,0,DM}$ remains the same between PDA08 and PDA13 and decreases with decreasing temperature

ACPD
15, 21671–21711, 2015

because observations show that nucleation on dust generally becomes more efficient at colder temperatures (e.g., Möhler et al., 2006; Field et al., 2006). PDA13 also uses an updated correlation for $S_{\mathrm{i,0,BC}}$, however, expressed in terms of surface polarity and organic coating:

$$S_{\mathrm{i,0}}^{\mathrm{BC}} = \widetilde{S}_{i,0} + \delta_0^1(F_{\mathrm{OC}}, F_{\mathrm{OC,0}}, F_{\mathrm{OC,1}}) \times \left[1.2 \times S_{\mathrm{i}}^{\mathrm{w}}(T) - \widetilde{S}_{i,0}\right] \quad (6)$$

where $\widetilde{S}_{i,0}$ is a baseline saturation ratio of 1.3, δ_0^1 is a cubic interpolation over organic coating, F_{OC}, between lower and upper bounds of $F_{\mathrm{OC,0}}$ and $F_{\mathrm{OC,1}}$ (Köhler et al., 2009; Crawford et al., 2011), and $S_{\mathrm{i}}^{\mathrm{w}}$ is the saturation ratio of vapor with respect to ice at exact water saturation, since minimal nucleation has been observed at water-subsaturated conditions for heavily-coated black carbon (DeMott et al., 1999). Surface polarity expresses hydrophilicity and is operationally defined as the number of water monolayers adsorbed to the aerosol surface at 50 % relative humidity, while the organic coating indicates the fraction of BC surface covered in insoluble organics. These parameters are source-dependent and difficult to determine, but this study assumes a high surface polarity of two monolayers and a low organic coating of 10 % to maximize any impact of black carbon (Table 1). Popovicheva et al. (2007) have also shown that these values describe aircraft engine combustion emissions, which would be relevant at this altitude.

The different aerosol contributing to INP concentrations, despite the same framework, can be understood by analyzing the expression for μ_X. Given that the same aerosol size and number distributions have been used in both runs (Table 1), the difference is in the active site density parameterization. The observationally-based terms making up the active site density are a threshold for water-subsaturated conditions, a threshold for warm sub-zero temperatures, and a background aerosol number (Hoose and Möhler, 2012):

$$n_{\mathrm{S,X}} = H_X(S_{\mathrm{i}}, T)\xi(T)\frac{\alpha_X N_{\mathrm{INP},*}}{\Omega_{X,*}} \quad (7)$$

ACPD
15, 21671–21711, 2015

Between PDA08 and PDA13, the reference surface area of dust increases from $\Omega_{DM,*} = 5\times10^{-7}\,m^2kg^{-1}$ to $\Omega_{DM,*} = 2\times10^{-6}\,m^2\,kg^{-1}$ and that of black carbon decreases from $\Omega_{BC,*} = 2.7\times10^{-7}\,m^2\,kg^{-1}$ to $\Omega_{BC,*} = 1\times10^{-7}\,m^2\,kg^{-1}$. This effect alone would yield a higher active site density for BC than dust. The portion of aerosol belonging to the BC group, α_{BC}, has also increased by 3 % in PDA13, and input temperatures are too low for the warm sub-zero temperature threshold, $\xi(T)$, to affect calculations. The difference in contributions, then, is the result of the water-subsaturated threshold, H_X. In PDA08, at higher supersaturations above about 40 %, the ice-nucleating portion of BC and mineral dust are both suppressed by 50 %, while in PDA13, BC nucleation is completely suppressed with the assumption that BC nucleation only occurs at water saturation, especially in the presence of coatings (Möhler et al., 2006). As a result, dust particles are the primary active INP for PDA13. Because the number concentration of dust is larger than that of BC, even in the Southern Hemisphere, the crystal number for PDA13 is higher in the Southern Hemisphere, as shown in Fig. 2. The review of Hoose and Möhler notes the suppression of ice nucleation by dust below water saturation for warmer sub-zero temperatures, as well as negative results for BC nucleation above 40 °C (Hoose and Möhler, 2012). But other studies have seen BC nucleation occur at water sub-saturated conditions and colder, cirrus-relevant temperatures (DeMott et al., 1999; Crawford et al., 2011). There is also the potential for immersion freezing within pores or cavities on the BC surface (Marcolli, 2014).

Surface polarity and organic coating parameters are currently prescribed and may be highly variable in the atmosphere. We have chosen a high polarity and low organic coating, so that BC contribution calculations represent an upper bound. For simulations with organic coating higher than 50 %, the INP contribution from BC disappears completely. Polarity and coating change with morphology and porosity, which change with source (Popovicheva et al., 2007). Given variable experimental results discussed above, a more detailed consideration of the BC emissions inventory would be needed to more accurately determine these parameters and BC contribution to crystal number.

ACPD
15, 21671–21711, 2015

3.3 Nucleation regime

The sign and magnitude of the insoluble aerosol number sensitivities, $\partial N_i/\partial N_{INP}$, can be used to elucidate the active freezing regime; an example is given in Fig. 4, which shows the annually-averaged sensitivity of N_i to accumulation mode dust number, $\partial N_i/\partial N_{dust,\,a}$, for all spectra. In the Southern Hemisphere, sensitivities for PDA08 are of small magnitude ($\mathcal{O}(10^{-4})$) and negative, as homogeneous nucleation dominates. There are localized regions of strong competitive nucleation in sub-Saharan Africa and northern South America, where sensitivities are of larger magnitude ($\mathcal{O}(10^{-3})$) and negative. Sensitivities throughout most of the Northern Hemisphere are of moderate magnitude and negative, indicating weaker competitive nucleation.

The PDA13 and CNT fields exhibit positive sensitivities throughout most of the Northern Hemisphere, indicating mostly heterogeneous nucleation. When updraft velocity is sufficiently large – over the Pacific Ocean, in the region of deep convection over Indonesia, or over the Himalayas or Rockies due to orographic lifting – a sufficiently high supersaturation may be generated to exceed the threshold for homogeneous nucleation and induce competitive nucleation. Regions of strong competitive nucleation appear for both spectra south of 60° S because dust, and hence INP, numbers are considerably lower than N_{lim}.

The magnitude of negative sensitivities during competitive nucleation reflect the threshold conditions assigned to a given aerosol group. The lower the threshold supersaturation for an aerosol group, the more readily it nucleates and the more effectively it depletes water vapor; this corresponds to larger magnitude $\partial N_i/\partial N_{dust,\,a}$ before N_{INP} surpasses N_{lim} and purely heterogeneous nucleation begins. PDA13 sensitivities to BC number are of larger magnitude than PDA08 values because $S_{i,0,BC}$ is lower for the polarity and F_{OC} values used here. The cusp of the INP-N_i trace becomes steeper, and the competition for water vapor is stronger in this case.

$\partial N_i/\partial N_{dust,\,a}$ is of large magnitude ($\mathcal{O}(10^{-2})$) and positive for the AIDA spectrum due to larger predicted INP numbers. These sensitivities decrease in magnitude over the

ACPD
15, 21671–21711, 2015

Antarctic because the active site density parameterization has a strong supersaturation dependence at cold temperatures (Fig. S1). If the temperature decreases by 5 K for a constant supersaturation, the active site density can drop by as much as 25 %. $\partial N_i/\partial N_{dust,\,a}$ also decreases in magnitude over Indonesia because the large updrafts here generate enough supersaturation that competitive nucleation occurs intermittently and reduces the annually-averaged magnitude of $\partial N_i/\partial N_{INP}$.

Along with these spatial patterns of annually-averaged sensitivity, we look at the time series, which show the frequency of occurrence of different nucleation regimes. Infrequent but large magnitude sensitivities can have an important influence on the annual average (Sheyko et al., 2015). Distributions of both accumulation mode dust number sensitivities and input updraft velocities are presented at (2.9° S, 135° E) over Indonesia and (0.95° N, 64° W) over northern South America in Fig. 5. These points are denoted by diamonds in Fig. 4. Their annually-averaged sensitivities differ significantly, despite their being in the same latitudinal band with similar aerosol loadings.

The location over Indonesia experiences high updraft more frequently, and the additional supersaturation generation translates to more competitive nucleation and larger magnitude sensitivities in PDA13, almost down to $-0.1\,L\,L^{-1}$. In PDA08, more supersaturation generation translates to more frequent homogeneous nucleation and smaller magnitude, less variable sensitivities, on the order of $10^{-3}\,L\,L^{-1}$. The location over South America has fewer instances of high updraft, so for PDA13, the system cannot always overcome the threshold supersaturation for homogeneous nucleation. Purely heterogeneous nucleation occurs more frequently: Fig. 5d has primarily positive sensitivities of small magnitude with an occasional large peak in N_i, which always corresponds to a large updraft. PDA08 exhibits stronger water vapor competition at this location, similar to the series in Fig. 5b. This behavior can be understood in terms of a transition along the INP-N_i trace in Fig. 1a: N_i and $\partial N_i/\partial N_{INP}$ respond differently to supersaturation generation based on how many INP the nucleation spectrum predicts.

ACPD
15, 21671–21711, 2015

3.4 INP nucleation efficiency

The positive values of $\partial N_i/\partial N_{INP}$ can be understood as a nucleation efficiency: those aerosol which act as efficient INP generate a large increase in crystal number for a given increase in aerosol number. In these simulations, accumulation mode dust has a mean efficiency of 0.0012 % in PDA08 and 0.079 % in PDA13, while coarse mode dust has a mean efficiency of 0.61 % in PDA08 and 0.078 % in PDA13. AIDA calculates considerably higher mean efficiency of 1.4 % for the accumulation mode and 52 % for the coarse mode. Black carbon in PDA08 is 0.03 % efficient on average, an order of magnitude higher than the accumulation mode dust. In PDA13, on the other hand, black carbon efficiency is an order lower than accumulation mode dust and skewed toward lower values (not shown). Efficiency of organic aerosol is negligible, on the order of 10^{-5}% and skewed to values as low as 10^{-12}%.

From Eq. (2) during purely heterogeneous nucleation,

$$\frac{\partial N_i}{\partial N_{INP,X}} = 1 - \exp(-n_s(S_i,T)\pi D^2) \quad (8)$$

As the number of embryos per aerosol particle becomes large, the nucleation-active fraction of the aerosol population, which is equivalent to the positive aerosol number sensitivity or the nucleation efficiency, approaches unity. This occurs because the product of active site density and aerosol surface area becomes large enough that an ice embryo should always form on the INP surface. Shifts in the number sensitivities reflect changing contributions to $N_{i,\,het}$. To illustrate, Fig. 6a shows the distribution of a random sample of 5000 daily-averaged dust number sensitivities, when ice nucleation is purely heterogeneous, i.e. $\partial N_i/\partial N_{INP} > 0$. The coarse mode dust number sensitivity is higher, and the accumulation mode dust sensitivity is lower for PDA08 than PDA13 because BC nucleation has been suppressed in the latter. The active site density of PDA08 BC is larger than that of dust under certain conditions (Fig. S1), meaning that BC efficiencies are higher than the accumulation mode dust efficiencies when aerosol diameter

ACPD
15, 21671–21711, 2015

for the two groups is assumed to be the same. The coarse mode sensitivities or efficiencies are even higher because their surface area is two orders of magnitude larger and outweighs a lower active site density.

The PDA08 distributions also have many more outliers because of the greater competition for water vapor between aerosol groups. The adjoint sensitivities are local in space and time, and in model grid cells without BC, dust in both modes is able to nucleate much more efficiently. In grid cells with more BC, the dust nucleation efficiency is significantly reduced because of the competition for water vapor between the two INP groups. The narrower range of AIDA efficiencies reinforces this point: this spectrum describes nucleation by dust in idealized conditions and no other aerosol compete for water vapor. Its active site parameterization also contains no threshold functions that abruptly reduce nucleation. For application in global models, it may be more effective to use parameterizations from experiments with multiple nucleating aerosol types.

Once an aerosol population has reached its maximum active fraction or efficiency, N_i becomes less sensitive to the number of these aerosol. In PDA13, the coarse mode dust population reaches an upper bound in its efficiency, and N_i sensitivity to coarse mode number decreases to a value comparable to the accumulation mode number sensitivity. For low active fractions, Eq. (8) can be linearized so that $f_{IN} \sim n_s(S_i,T)D^2$. Given that $n_s \sim \mathcal{O}(10^9\,m^{-2})$ and $D \sim \mathcal{O}(10^{-6}$ m) in the coarse mode, the maximum active fraction is expected to be on the order of 10^{-3}, which is indeed the value seen in Fig. 6.

3.5 Size sensitivity and the active site density

Diameter sensitivities can also be understood in terms of nucleation regime. When nucleation is purely heterogeneous, diameter sensitivity is positive; increasing aerosol diameter increases crystal number because for a given active site density, more surface area increases the number of ice embryos per aerosol. During competitive nucleation, diameter sensitivity becomes negative, as more available surface area for heteroge-

ACPD
15, 21671–21711, 2015

neous nucleation reduces N_i from $N_{i,\,hom}$. As with number sensitivity, the magnitude of negative diameter sensitivities reflects how intensely a certain aerosol group can deplete water vapor. The magnitude of positive diameter sensitivities is larger for coarse mode than accumulation mode dust in all spectra (Fig. 6); an incremental increase in diameter generates more surface area for larger particles than for smaller particles.

The magnitude of positive diameter sensitivities also reflects active site density. From Eq. (2), during purely heterogeneous nucleation,

$$\frac{\partial N_i}{\partial D} = 2\pi D n_X n_s(S_i,T)\ \exp(-n_s(S_i,T)\pi D^2) \tag{9}$$

which shows that $\partial N_i/\partial D \propto D\exp(-D^2)$ and $\partial N_i/\partial D \propto n_s\exp(-n_s)$. The magnitude of diameter sensitivity first increases, then decreases, with diameter. The larger the diameter, the faster the sensitivity decreases after its maximum and the larger that maximum sensitivity. Again for active site density, the magnitude of diameter sensitivity first increases then decreases with n_s. And the larger the active site density, the faster the sensitivity decreases after reaching its maximum value. The first effect is stronger because $\partial N_i/\partial D$ is proportional to the exponential of active site density but to the exponential of diameter squared.

Figure 6b is constructed again from a random sample of 5000 daily-averaged dust diameter sensitivities in the purely heterogeneous regime, i.e. $\partial N_i/\partial D > 0$. The accumulation mode diameter sensitivity reaches higher values than the coarse mode diameter sensitivity for PDA13 and AIDA because the higher number of accumulation mode dust particles outweighs the larger coarse mode surface area. The AIDA and PDA13 spectra also reach the same maximum diameter sensitivities (10^{11} µm cm^{-3} in the coarse mode) as both have reached their maximum active fraction. These features do not characterize the PDA08 distributions because of competition for water vapor with black carbon. Given the higher active site density and equal surface area of black carbon relative to accumulation mode dust, $\partial N_i/\partial D_{dust,\,a}$ is smaller in PDA08 than in the other spectra. The surface area increase from the addition of a coarse mode dust

ACPD
15, 21671–21711, 2015

particle outweighs the higher BC active site density and $\partial N_i/\partial D_{dust,\,c}$ in PDA08 is comparable to the values in the other spectra. In summary, spectra with large active site densities will be highly sensitive to aerosol diameter over a limited range of these diameters, while spectra with lower active site densities will be less sensitive to aerosol diameter but over a larger range of these diameters. These trends may be convoluted by competition for water vapor with other aerosol species.

3.6 Sensitivity of N_i to temperature and sulfate aerosol

The above discussion has focused on insoluble aerosol sensitivities. Soluble aerosol sensitivities, $\partial N_i/\partial N_{sulf}$, are always positive because the addition of these soluble particles enhance homogeneous nucleation and crystal number, regardless of the insoluble INP profile. When purely heterogeneous nucleation occurs, $\partial N_i/\partial N_{sulf}$ is zero. These fields have not changed in magnitude between spectra because the treatment of homogeneous nucleation is identical in all cases. Sulfate sensitivity has the largest magnitude when the homogeneously-formed fraction is largest.

Temperature sensitivities, $\partial N_i/\partial T$, are generally negative because colder temperatures tend to facilitate ice nucleation. An increase in temperature may exceed the threshold temperature for a certain aerosol group, deactivating it, and allowing homogeneous nucleation to generate a larger N_i. This phenomenon can be observed for both PDA08 and PDA13 fields, in which positive sensitivities fall exclusively at the outflow of Saharan dust around the equator where input temperature is between 225 and 230 K. These temperatures are in the range at which the water-subsaturated threshold function for dust drops ($T_0^{DM} = -40\,^{\circ}C$ and $\Delta T = 5\,^{\circ}C$), so that the primary contributor to heterogeneous nucleation depletes less water vapor and homogeneous nucleation yields higher N_i.

The magnitude of $\partial N_i/\partial T$ is smaller than expected from classical nucleation theory, probably due to compensating effects. For example, as temperature increases so does water vapor diffusivity, which enhances crystal growth and reduces number. But latent heat of sublimation also increases as temperature drops, which slows the ice

ACPD
15, 21671–21711, 2015

crystal growth rate. The homogeneous nucleation coefficient increases orders of magnitude with lower temperatures (Koop et al., 2000). The threshold supersaturation for dust, however, also goes down, so that deposition nucleation can more easily inhibit homogeneous nucleation. These temperature dependencies may counterbalance and explain the intermediate regime noted by Hoose and Möhler, in which n_s isolines are independent of temperature and driven primarily by supersaturation (Hoose and Möhler, 2012).

4 Summary

Thorough understanding of nucleated ice crystal variability in global simulations will help improve model representation of cirrus clouds and their radiative forcing. Towards this end, adjoint sensitivity analysis provides a powerful and efficient means of quantifying the prevalent ice nucleation regime, active site density and inputs driving temporal and spatial variability in the model output. From analysis of a single GCM simulation for each nucleation spectrum, using CAM 5.1 and current day emissions, we have shown the following results:

– *Nucleation regime is determined by INP, but N_i is determined by threshold conditions and INP abundance.* During a simulation, the number of ice-nucleating particles predicted by a nucleation spectrum determines its nucleation regime, or equivalently where the system "sits" along the INP-N_i trace. Threshold supersaturation and the number of INP relative to the limiting number determine the nucleated ice crystal number. Lower ice crystal numbers can be calculated in spite of higher INP, if certain aerosol have less stringent threshold supersaturations, because $s_{i,0,X}$ affects the steepness and depth of the competitive cusp on the INP-N_i trace. At the coldest temperatures, strong supersaturation dependence of active site parameterizations may also reduce N_i. In addition, the number of INP only dictates ice crystal number relative to the limiting number to prevent homogeneous nucleation in this framework. If N_{lim} calculated in one spectrum is lower

ACPD
15, 21671–21711, 2015

relative to another, this spectrum may still calculate higher crystal number with fewer ice-nucleating particles.

– *Black carbon nucleation can be suppressed in models with a water-subsaturated threshold function. The suppression of certain INP groups manifests as shifts in the aerosol number sensitivity distributions.* Dust contribution to heterogeneously-formed number dominates on a global scale for PDA13 runs. Deconstructing the active site density parameterization shows that this suppression is due to a more stringent water-subsaturated threshold function for black carbon. Although the surface polarity and organic coating parameters remain unconstrained, we have chosen values which would maximize the black carbon ice-nucleating activity. The model predicts that black carbon contribution is negligible to N_i at this pressure level, if the PDA13 treatment is not too conservative.

  Differing aerosol contributions to N_i manifest in the number sensitivity distributions. When black carbon cannot act as an INP and there is no competition for water vapor between aerosol types, the sensitivity to accumulation mode dust number increases and the sensitivity to coarse mode dust number decreases. Glassy aerosol has a small, but regionally important and seasonally-dependent contribution in PDA13.

– *The sign of ice crystal number sensitivity to insoluble aerosol number or diameter indicates nucleation regime.* When insoluble aerosol number or diameter sensitivities are small and negative, nucleation is predominantly homogeneous. When these values become large and negative, competitive nucleation has initiated, and when the values become positive, nucleation is purely heterogeneous. The spatial distributions of insoluble aerosol number sensitivity, as in Fig. 4, can help explain those of crystal number in Fig. 2. Temporal distributions of sensitivity can also be used to understand regime shifts along the INP-N_i trace. Spectra that predict different INP numbers may respond differently to additional supersaturation generation.

ACPD
15, 21671–21711, 2015

– *The magnitude of positive aerosol number sensitivity reflects heterogeneous nucleation efficiency. The sensitivity of positive diameter sensitivity reflects active site density.* When nucleation is purely heterogeneous, the magnitude of aerosol number sensitivity can be understood as a nucleation efficiency. The range of efficiencies is limited when there is no competition for water vapor between aerosol groups. Crystal number is more sensitive to the aerosol species with higher associated surface areas, until those species reach their maximum active fractions. In the same manner, crystal number is more sensitive to the size of larger aerosol, until the maximum active fraction is obtained. An incremental increase in the diameter of a large particle yield greater surface area but exhausts the active site density more quickly.

– *Temperature sensitivities are of smaller magnitude than expected with classical nucleation theory because of compensating temperature dependencies.* Limited sensitivities to temperature reflect the empirically observed "intermediate temperature regime," where supersaturation is more influential on nucleation.

The Supplement related to this article is available online at doi:10.5194/acpd-15-21671-2015-supplement.

Acknowledgements. This work was made possible through support from DOE EaSM. SS gratefully acknowledges support from a National Aeronautics and Space Administration Earth and Space Science Fellowship.

References

Barahona, D.: On the ice nucleation spectrum, Atmos. Chem. Phys., 12, 3733–3752, doi:10.5194/acp-12-3733-2012, 2012. 21673

ACPD
15, 21671–21711, 2015

Barahona, D. and Nenes, A.: Parameterization of cirrus cloud formation in large-scale models: Homogeneous nucleation, J. Geophys. Res., 113, 2156–2202, doi:10.1029/2007JD009355, 2008. 21673, 21677

Barahona, D. and Nenes, A.: Parameterizing the competition between homogeneous and heterogeneous freezing in cirrus cloud formation – monodisperse ice nuclei, Atmos. Chem. Phys., 9, 369–381, doi:10.5194/acp-9-369-2009, 2009a. 21673, 21677, 21681

Barahona, D. and Nenes, A.: Parameterizing the competition between homogeneous and heterogeneous freezing in ice cloud formation – polydisperse ice nuclei, Atmos. Chem. Phys., 9, 5933–5948, doi:10.5194/acp-9-5933-2009, 2009b. 21673, 21674, 21677, 21680, 21703

Barahona, D. and Nenes, A.: Dynamical states of low temperature cirrus, Atmos. Chem. Phys., 11, 3757–3771, doi:10.5194/acp-11-3757-2011, 2011. 21682

Barahona, D., Rodriguez, J., and Nenes, A.: Sensitivity of the global distribution of cirrus ice crystal concentration to heterogeneous freezing, J. Geophys. Res., 115, 3757–3771, doi:10.1029/2010JD014273, 2010. 21674, 21676, 21683

Barahona, D., Molod, A., Bacmeister, J., Nenes, A., Gettelman, A., Morrison, H., Phillips, V., and Eichmann, A.: Development of two-moment cloud microphysics for liquid and ice within the NASA Goddard Earth Observing System Model (GEOS-5), Geosci. Model Dev., 7, 1733–1766, doi:10.5194/gmd-7-1733-2014, 2014. 21703

Boucher, O., Randall, D., Artaxo, P., Bretherton, C., Feingold, G., Forster, P., Kerminen, V.-M., Kondo, Y., Liao, H., Lohmann, U., Rasch, P., Sathessh, S., Sherwood, S., Stevens, B., and Zhang, X.: Clouds and aerosols, in: Climate Change 2013: The Physical Science Basis. Contribution of Working Group I to the Fifth Assessment Report of the Intergovernmental Panel on Climate Change, Cambridge University Press, Cambridge, UK, and New York, NY, USA, 571–657, 2013. 21672

Broadley, S. L., Murray, B. J., Herbert, R. J., Atkinson, J. D., Dobbie, S., Malkin, T. L., Condliffe, E., and Neve, L.: Immersion mode heterogeneous ice nucleation by an illite rich powder representative of atmospheric mineral dust, Atmos. Chem. Phys., 12, 287–307, doi:10.5194/acp-12-287-2012, 2012. 21675

Capps, S. L., Henze, D. K., Hakami, A., Russell, A. G., and Nenes, A.: ANISORROPIA: the adjoint of the aerosol thermodynamic model ISORROPIA, Atmos. Chem. Phys., 12, 527–543, doi:10.5194/acp-12-527-2012, 2012. 21676

ACPD
15, 21671–21711, 2015

Chen, J.-P., Hazra, A., and Levin, Z.: Parameterizing ice nucleation rates using contact angle and activation energy derived from laboratory data, Atmos. Chem. Phys., 8, 7431–7449, doi:10.5194/acp-8-7431-2008, 2008. 21703

Connolly, P. J., Möhler, O., Field, P. R., Saathoff, H., Burgess, R., Choularton, T., and Gallagher, M.: Studies of heterogeneous freezing by three different desert dust samples, Atmos. Chem. Phys., 9, 2805–2824, doi:10.5194/acp-9-2805-2009, 2009. 21675

Cox, S. J., Kathmann, S. M., Slater, B., and Michaelides, A.: Molecular simulations of heterogeneous ice nucleation. I. Controlling ice nucleation through surface hydrophilicity, J. Chem. Phys., 142, 184704, doi:10.1063/1.4919714, 2015. 21673

Crawford, I., Möhler, O., Schnaiter, M., Saathoff, H., Liu, D., McMeeking, G., Linke, C., Flynn, M., Bower, K. N., Connolly, P. J., Gallagher, M. W., and Coe, H.: Studies of propane flame soot acting as heterogeneous ice nuclei in conjunction with single particle soot photometer measurements, Atmos. Chem. Phys., 11, 9549–9561, doi:10.5194/acp-11-9549-2011, 2011. 21685, 21686

Curry, J. A. and Khvorostyanov, V. I.: Assessment of some parameterizations of heterogeneous ice nucleation in cloud and climate models, Atmos. Chem. Phys., 12, 1151–1172, doi:10.5194/acp-12-1151-2012, 2012. 21675, 21683

d'Almeida, G.: On the variability of desert aerosol radiative characteristics, J. Geophys. Res., 92, 3017–3026, doi:10.1029/JD092iD03p03017, 1987. 21703

DeMott, P., Chen, Y., Kreidenweis, S., Rogers, D., and Sherman, D.: Ice formation by black carbon particles, Geophys. Res. Letters, 26, 2429–2432, doi:10.1029/1999GL900580, 1999. 21685, 21686

Dentener, F., Kinne, S., Bond, T., Boucher, O., Cofala, J., Generoso, S., Ginoux, P., Gong, S., Hoelzemann, J. J., Ito, A., Marelli, L., Penner, J. E., Putaud, J.-P., Textor, C., Schulz, M., van der Werf, G. R., and Wilson, J.: Emissions of primary aerosol and precursor gases in the years 2000 and 1750 prescribed data-sets for AeroCom, Atmos. Chem. Phys., 6, 4321–4344, doi:10.5194/acp-6-4321-2006, 2006. 21703

Errico, R. M.: What is an adjoint model?, B. Am. Meteol. Soc., 78, 2577–2591, doi:10.1175/1520-0477(1997)078<2577:WIAAM>2.0.CO;2, 1997. 21676

Field, P. R., Möhler, O., Connolly, P., Krämer, M., Cotton, R., Heymsfield, A. J., Saathoff, H., and Schnaiter, M.: Some ice nucleation characteristics of Asian and Saharan desert dust, Atmos. Chem. Phys., 6, 2991–3006, doi:10.5194/acp-6-2991-2006, 2006. 21685, 21703

ACPD
15, 21671–21711, 2015

Gettelman, A., Randel, W., Wu, F., and Massie, S.: Transport of water vapor in the tropical tropopause layer, Geophys. Res. Letters, 29, 9-1–9-4, doi:10.1029/2001GL013818, 2002. 21672
Giering, R. and Kaminski, T.: Recipes for adjoint code construction, ACM T. Math. Software, 24, 437–474, doi:10.1145/293686.293695, 1998. 21676
Hakami, A., Henze, D., Seinfeld, J., Singh, K., Sandu, A., Kim, S., Byun, D., and Li, Q.: The adjoint of CMAQ, Environ. Sci. Technol., 41, 7807–7817, doi:10.1021/es070944p, 2007. 21676
Hascoët, L. and Pascual, V.: TAPENADE 2.1 User's Guide, INRIA Technical Report RT-0300, French Institute for Research in Computer Science and Automation, Sophia Antipolis, France, p. 78, 2004. 21677
Hiranuma, N., Paukert, M., Steinke, I., Zhang, K., Kulkarni, G., Hoose, C., Schnaiter, M., Saathoff, H., and Möhler, O.: A comprehensive parameterization of heterogeneous ice nucleation of dust surrogate: laboratory study with hematite particles and its application to atmospheric models, Atmos. Chem. Phys., 14, 13145–13158, doi:10.5194/acp-14-13145-2014, 2014. 21675, 21680
Hoose, C. and Möhler, O.: Heterogeneous ice nucleation on atmospheric aerosols: a review of results from laboratory experiments, Atmos. Chem. Phys., 12, 9817–9854, doi:10.5194/acp-12-9817-2012, 2012. 21685, 21686, 21693, 21703
Kärcher, B. and Lohmann, U.: A Parameterization of cirrus cloud formation: Homogeneous freezing including effects of aerosol size, J. Geophys. Res., 107, 2156–2202, doi:10.1029/2001JD001429, 2002. 21674
Karydis, V. A., Capps, S. L., Russell, A. G., and Nenes, A.: Adjoint sensitivity of global cloud droplet number to aerosol and dynamical parameters, Atmos. Chem. Phys., 12, 9041–9055, doi:10.5194/acp-12-9041-2012, 2012. 21676
Köhler, K. A., DeMott, P. J., Kreidenweis, S. M., Popovicheva, O. B., Petters, M. D., Carrico, C. M., Kireeva, E. D., Khokhlova, T. D., and Shonija, N. K.: Cloud condensation nuclei and ice nucleation activity of hydrophobic and hydrophilic soot particles, Phys. Chem. Chem. Phys., 11, 7906–7920, doi:10.1039/B905334B, 2009. 21685
Koop, T., Luo, B., Tsias, A., and Peter, T.: Water activity as the determinant for homogeneous ice nucleation in aqueous solutions, Nature, 406, 611–614, doi:10.1038/35020537, 2000. 21693
Krämer, M., Schiller, C., Afchine, A., Bauer, R., Gensch, I., Mangold, A., Schlicht, S., Spelten, N., Sitnikov, N., Borrmann, S., de Reus, M., and Spichtinger, P.: Ice supersaturations

ACPD
15, 21671–21711, 2015

and cirrus cloud crystal numbers, Atmos. Chem. Phys., 9, 3505–3522, doi:10.5194/acp-9-3505-2009, 2009. 21682
Kulkarni, G., Fan, J., Comstock, J. M., Liu, X., and Ovchinnikov, M.: Laboratory measurements and model sensitivity studies of dust deposition ice nucleation, Atmos. Chem. Phys., 12, 7295–7308, doi:10.5194/acp-12-7295-2012, 2012. 21673
Lamarque, J.-F., Bond, T. C., Eyring, V., Granier, C., Heil, A., Klimont, Z., Lee, D., Liousse, C., Mieville, A., Owen, B., Schultz, M. G., Shindell, D., Smith, S. J., Stehfest, E., Van Aardenne, J., Cooper, O. R., Kainuma, M., Mahowald, N., McConnell, J. R., Naik, V., Riahi, K., and van Vuuren, D. P.: Historical (1850–2000) gridded anthropogenic and biomass burning emissions of reactive gases and aerosols: methodology and application, Atmos. Chem. Phys., 10, 7017–7039, doi:10.5194/acp-10-7017-2010, 2010. 21678
Lin, R.-F., Starr, D. O., Reichardt, J., and DeMott, P. J.: Nucleation in synoptically forced cirrostratus, J. Geophys. Res., 110, D08208, doi:10.1029/2004JD005362, 2005. 21673
Liu, X. and Penner, J.: Ice nucleation parameterization for global models, Meteorol. Z., 14, 499–514, doi:10.1127/0941-2948/2005/0059, 2005. 21674
Liu, X., Easter, R. C., Ghan, S. J., Zaveri, R., Rasch, P., Shi, X., Lamarque, J.-F., Gettelman, A., Morrison, H., Vitt, F., Conley, A., Park, S., Neale, R., Hannay, C., Ekman, A. M. L., Hess, P., Mahowald, N., Collins, W., Iacono, M. J., Bretherton, C. S., Flanner, M. G., and Mitchell, D.: Toward a minimal representation of aerosols in climate models: description and evaluation in the Community Atmosphere Model CAM5, Geosci. Model Dev., 5, 709–739, doi:10.5194/gmd-5-709-2012, 2012a. 21678
Liu, X., Shi, X., Zhang, K., Jensen, E. J., Gettelman, A., Barahona, D., Nenes, A., and Lawson, P.: Sensitivity studies of dust ice nuclei effect on cirrus clouds with the Community Atmosphere Model CAM5, Atmos. Chem. Phys., 12, 12061–12079, doi:10.5194/acp-12-12061-2012, 2012b. 21684
Lupi, L., Hudait, A., and Molinero, V.: Heterogeneous nucleation of ice on carbon surfaces, J. Am. Chem. Soc., 136, 3156–3164, doi:10.1021/ja411507a, 2014. 21673
Marcolli, C.: Deposition nucleation viewed as homogeneous or immersion freezing in pores and cavities, Atmos. Chem. Phys., 14, 2071–2104, doi:10.5194/acp-14-2071-2014, 2014. 21686
Marcolli, C., Gedamke, S., Peter, T., and Zobrist, B.: Efficiency of immersion mode ice nucleation on surrogates of mineral dust, Atmos. Chem. Phys., 7, 5081–5091, doi:10.5194/acp-7-5081-2007, 2007. 21674

ACPD
15, 21671–21711, 2015

Meyers, M., DeMott, P., and Cotton, R.: New primary ice-nucleation parameterization in an explicit cloud model, J. Appl. Meteorol., 31, 708–721, doi:10.1175/1520-0450(1992)031<0708:NPINPI>2.0.CO;2, 1992. 21674

Möhler, O., Field, P. R., Connolly, P., Benz, S., Saathoff, H., Schnaiter, M., Wagner, R., Cotton, R., Krämer, M., Mangold, A., and Heymsfield, A. J.: Efficiency of the deposition mode ice nucleation on mineral dust particles, Atmos. Chem. Phys., 6, 3007–3021, doi:10.5194/acp-6-3007-2006, 2006. 21685, 21686

Morales Betancourt, R. and Nenes, A.: Understanding the contributions of aerosol properties and parameterization discrepancies to droplet number variability in a global climate model, Atmos. Chem. Phys., 14, 4809–4826, doi:10.5194/acp-14-4809-2014, 2014. 21678

Morales Betancourt, R., Lee, D., Oreopoulos, L., Sud, Y. C., Barahona, D., and Nenes, A.: Sensitivity of cirrus and mixed-phase clouds to the ice nuclei spectra in McRAS-AC: single column model simulations, Atmos. Chem. Phys., 12, 10679–10692, doi:10.5194/acp-12-10679-2012, 2012. 21676, 21683

Niedermeier, D., Hartmann, S., Shaw, R. A., Covert, D., Mentel, T. F., Schneider, J., Poulain, L., Reitz, P., Spindler, C., Clauss, T., Kiselev, A., Hallbauer, E., Wex, H., Mildenberger, K., and Stratmann, F.: Heterogeneous freezing of droplets with immersed mineral dust particles – measurements and parameterization, Atmos. Chem. Phys., 10, 3601–3614, doi:10.5194/acp-10-3601-2010, 2010. 21675

Niemand, M., Möhler, O., Vogel, B., Vogel, H., and Hoose, C.: A particle-surface-area-based parameterization of immersion freezing on desert dust particles, J. Atmos. Sci., 69, 3077–3092, doi:10.1175/JAS-D-11-0249.1, 2012. 21674, 21675

Phillips, V., DeMott, P., and Andronache, C.: An empirical parameterization of heterogeneous ice nucleation for multiple chemical species of aerosol, J. Atmos. Sci., 65, 2757–2783, doi:10.1175/2007JAS2546.1, 2008. 21675

Phillips, V., DeMott, P., Andronache, C., Pratt, K., Prather, K., Subramanian, R., and Twohy, C.: Improvements to an empirical parameterization of heterogeneous ice nucleation and its comparison with observations, J. Atmos. Sci., 70, 378–409, doi:10.1175/JAS-D-12-080.1, 2013. 21679

Popovicheva, O., Persiantseva, N., Shonija, N., DeMott, P., Koehler, K., Petters, M., Kreidenweis, S., Tishkova, V., Demirdjian, B., and Suzanne, J.: Water interaction with hydrophobic and hydrophilic soot particles, Phys. Chem. Chem. Phys., 10, 2332–2344, doi:10.1039/b718944n, 2007. 21686, 21703

ACPD
15, 21671–21711, 2015

Prenni, A., Harrington, J., Tjernström, M., DeMott, P., Avramov, A., Long, C., Kreidenweis, S., Olsson, P., and Verlinde, J.: Can ice-nucleating aerosols affect arctic seasonal climate?, B. Am. Meteol. Soc., 88, 541–550, doi:10.1175/BAMS-88-4-541, 2007. 21675

Pruppacher, H. and Klett, J.: Microphysics of Clouds and Precipitation, 2nd edn., Kluwer Academic Publishers, Boston, MA, 1997. 21673

Reinhardt, A. and Doye, J. P. K.: Effects of surface interactions on heterogeneous ice nucleation for a monatomic water model, J. Chem. Phys., 141, 084501, doi:10.1063/1.4892804, 2014. 21673

Ren, C. and MacKenzie, A.: Cirrus parameterization and the role of ice nuclei, Q. J. Roy. Meteor. Soc., 131, 1585–1605, doi:10.1256/qj.04.126, 2005. 21681

Savre, J., Ekman, A., Svensson, G., and Tjernström, M.: Parameterizing ice nucleation ability of mineral dust particles in the deposition mode: numerical investigations using large eddy simulation, AIP Conf. Proc., 922, 922–925, doi:10.1063/1.4803422, 2013. 21674

Sheyko, B., Sullivan, S. C., Morales-Betancourt, R., Capps, S., Barahona, D., Shi, X., Liu, X., and Nenes, A.: Quantifying sensitivities of ice crystal number and sources of ice crystal number variability in CAM 5.1 using the adjoint of a physically based cirrus formation parameterization, J. Geophys. Res., 120, 2834–2854, doi:10.1002/2014JD022457, 2015. 21676, 21677, 21688

Skrotzki, J., Connolly, P., Schnaiter, M., Saathoff, H., Möhler, O., Wagner, R., Niemand, M., Ebert, V., and Leisner, T.: The accommodation coefficient of water molecules on ice – cirrus cloud studies at the AIDA simulation chamber, Atmos. Chem. Phys., 13, 4451–4466, doi:10.5194/acp-13-4451-2013, 2013. 21703

Spichtinger, P. and Krämer, M.: Tropical tropopause ice clouds: a dynamic approach to the mystery of low crystal numbers, Atmos. Chem. Phys., 13, 9801–9818, doi:10.5194/acp-13-9801-2013, 2013. 21682

Steinke, I., Hoose, C., Möhler, O., Connolly, P., and Leisner, T.: A new temperature- and humidity-dependent surface site density approach for deposition ice nucleation, Atmos. Chem. Phys., 15, 3703–3717, doi:10.5194/acp-15-3703-2015, 2015. 21679

Vali, G.: Interpretation of freezing nucleation experiments: singular and stochastic; sites and surfaces, Atmos. Chem. Phys., 14, 5271–5294, doi:10.5194/acp-14-5271-2014, 2014. 21673

Wang, Y., Liu, X., Hoose, C., and Wang, B.: Different contact angle distributions for heterogeneous ice nucleation in the Community Atmospheric Model version 5, Atmos. Chem. Phys., 14, 10411–10430, doi:10.5194/acp-14-10411-2014, 2014. 21674

ACPD
15, 21671–21711, 2015

Whitby, K.: The physical characteristics of sulfur aerosols, Atmos. Environ., 41, 25–49, doi:10.1016/0004-6981(78)90196-8, 2007. 21703

Xie, S., Liu, X., Zhao, C., and Zhang, Y.: Sensitivity of CAM5-simulated Arctic clouds and radiation to nucleation parameterization, J. Climate, 26, 5981–5999, doi:10.1175/JCLI-D-12-00517.1, 2013. 21675

Zuberi, B., Bertram, A., Cassa, C., Molina, L., and Molina, M.: Heterogeneous nucleation of ice in ammonium sulfate-water particles with mineral dust immersions, Geophys. Res. Lett., 29, 1944–8007 , doi:10.1029/2001GL014289, 2002. 21684

ACPD

15, 21671–21711, 2015

Table 1. Adjustable parameters for ABN15 simulations.

Parameter		Value	Citation
Pressure level		232 hPa	ISCCP
Deposition coefficient	α	0.7	Skrotzki et al. (2013)
Width of BC SD	σ_{BC}	1.8	Dentener et al. (2006)
Width of dust SDs	σ_{DM}	1.6	d'Almeida (1987); Field et al. (2006)
Width of organic SD	σ_{org}	1.8	Dentener et al. (2006)
Width of sulfate SD	σ_{sulf}	2.3	Whitby (2007)
Liquid mixing ratio	q_c	1×10^{-6} kg kg^{-1}	Barahona et al. (2014)
Surface polarity	P_s	2	Popovicheva et al. (2007)
Organic coating	F_{oc}	10 %	Popovicheva et al. (2007)
Threshold supersaturation for dust	$S_{i,0,DM}$	20 %	Hoose and Möhler (2012)
Threshold supersaturation for black	$S_{i,0,BC}$	35 %	Hoose and Möhler (2012)
Maximum nucleation efficiency of dust	e_{DM}	50 %	Barahona and Nenes (2009b)
Effective contact angle for dust	θ_{DM}	16°	Chen et al. (2008)
Maximum nucleation efficiency of black carbon	e_{BC}	2 %	Barahona and Nenes (2009b)
Effective contact angle for black carbon	θ_{BC}	40°	Chen et al. (2008)

ACPD
15, 21671–21711, 2015

Table 2. Range of predicted ice-nucleating particle numbers and abundances for different nucleation spectra.

Spectrum	INP range [L^{-1}]	Median INP number [L^{-1}]	Interquartile range of INP number [L^{-1}]	A_{INP} range	Median A_{INP}	Interquartile range of A_{INP}
PDA08	0.047–5.07	0.48	1.05	0.0070–11.11	0.34	0.62
PDA13	0.57–28.6	3.60	10.56	0.67–49.37	10.25	10.02
CNT	6.94–1270.47	50.38	169.82	0.97–7220.64	20.80	36.52
AIDA	3.60–855.36	52.51	190.49	4.02–4549.94	20.47	24.35

ACPD
15, 21671–21711, 2015

Table A1. Notation.

BN09	Barahona and Nenes (2009) cirrus formation parameterization
$N_{\mathrm{i,\,het}}$	Heterogeneously-formed ice crystal number
INP	Ice-nucleating particles
s_{i}	Supersaturation of water vapor with respect to ice
PDA08	Phillips, DeMott, and Andromache 2008 INP spectrum
PDA13	Phillips et al. INP spectrum, updated from 2008
AIDA	Heterogeneous INP spectra derived from Aerosol Interaction and Dynamics in the Atmosphere cloud chamber data
$N_{\mathrm{i,\,het}}$	Number of heterogeneously-nucleated ice crystals
$N_{\mathrm{i,\,hom}}$	Number of homogeneously-nucleated ice crystals
N_{lim}	Limiting number of INP to prevent homogeneous nucleation
s_{max}	Maximum supersaturation which develops within the cloud parcel
s_{hom}	Threshold supersaturation for homogeneous nucleation
S_{i}	Saturation ratio of water vapor with respect to ice
μ_X	Number of ice embryos per aerosol surface
$\partial N_{\mathrm{i}}/\partial D_{\mathrm{dust,\,c}}$	Nucleated ice crystal number sensitivity to coarse mode dust diameter
$\partial N_{\mathrm{i}}/\partial D_{\mathrm{dust,\,a}}$	Nucleated ice crystal number sensitivity to accumulation mode dust diameter
$\partial N_{\mathrm{i}}/\partial N_{\mathrm{dust,\,a}}$	Nucleated ice crystal number sensitivity to accumulation mode dust number
$\partial N_{\mathrm{i}}/\partial N_{\mathrm{INP},X}$	Nucleated ice crystal number sensitivity to INP number in group X

ACPD
15, 21671–21711, 2015

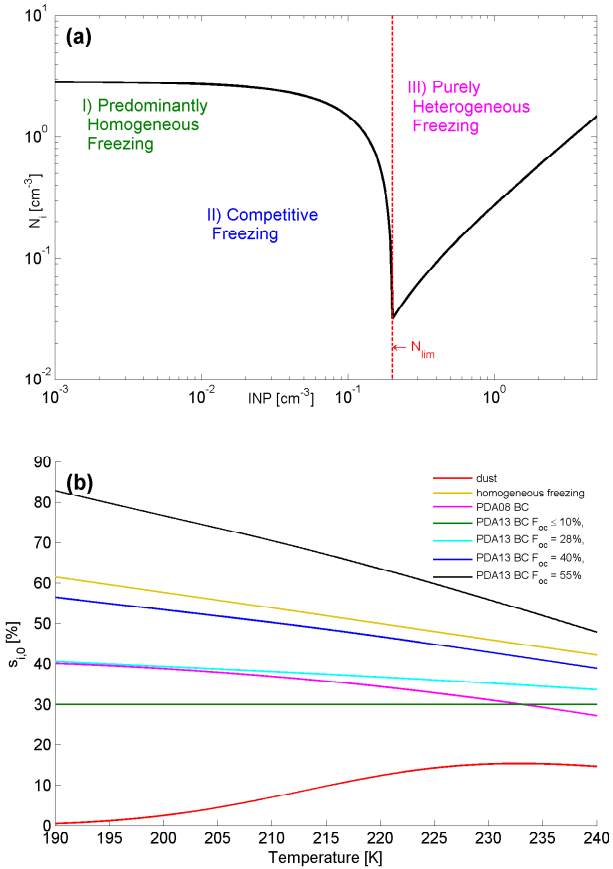

Figure 1. (a) Freezing regimes of cirrus in the INP-ice crystal number space; **(b)** threshold supersaturations for homogeneous freezing and heterogeneous nucleation of mineral dust and BC with different organic coatings.

ACPD
15, 21671–21711, 2015

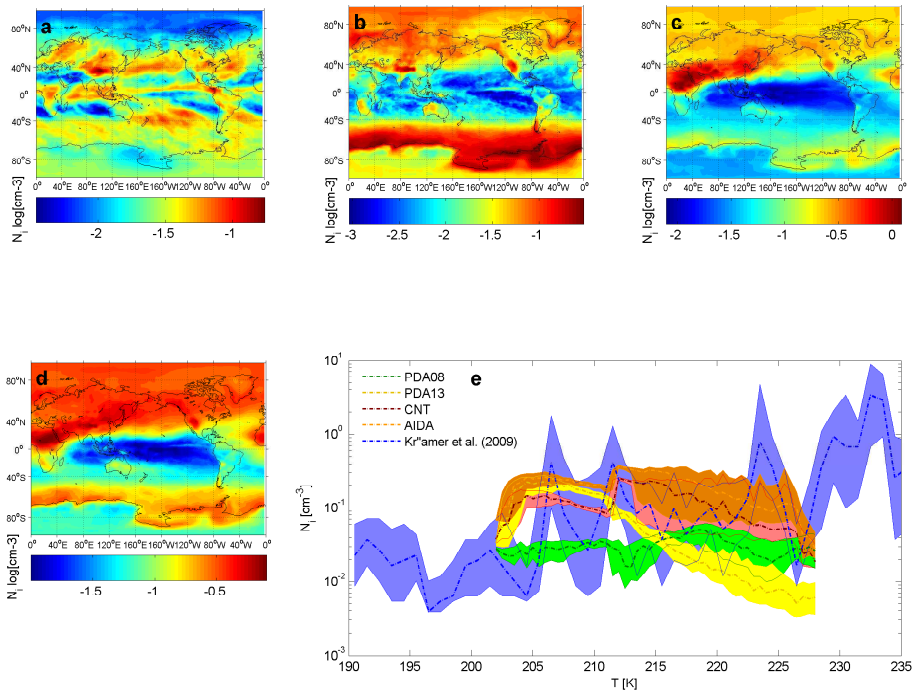

Figure 2. Annually-averaged output nucleated ice crystal number, N_i from the cirrus formation parameterization for **(a)** PDA08, **(b)** PDA13, **(c)** CNT, **(d)** AIDA spectra; and **(e)** comparison of these values with crystal number measurements from Krämer et al. (2009), where the envelope represents first and third quartiles for 0.5 K bins.

ACPD
15, 21671–21711, 2015

Understanding N_i variability for different INP spectra

S. C. Sullivan et al.

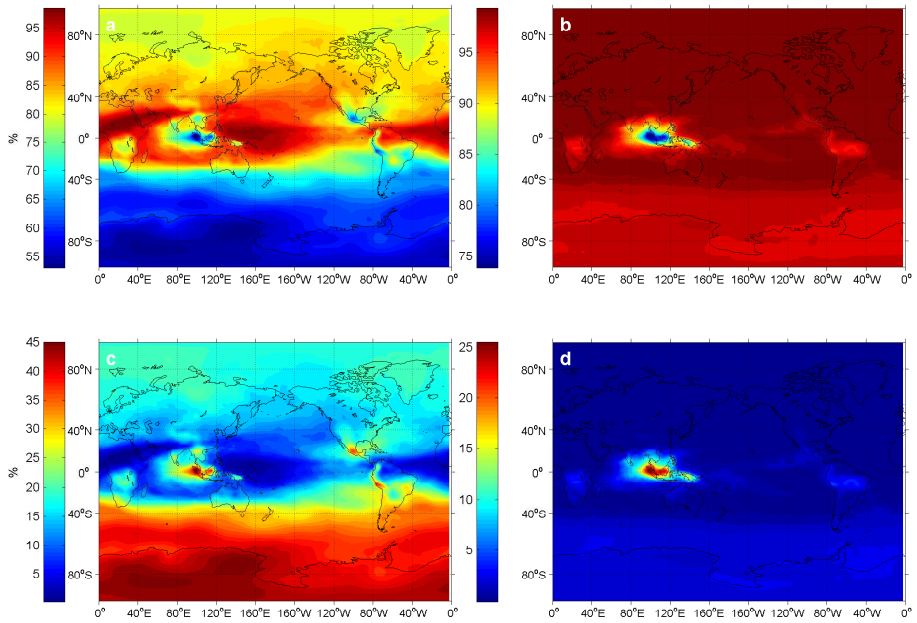

Figure 3. Annually-averaged contributions of dust and BC to heterogeneously-formed ice crystal number. **(a)** Dust contribution in PDA08; **(b)** dust contribution in PDA13; **(c)** black carbon contribution in PDA08; and **(d)** black carbon contribution in PDA13.

ACPD
15, 21671–21711, 2015

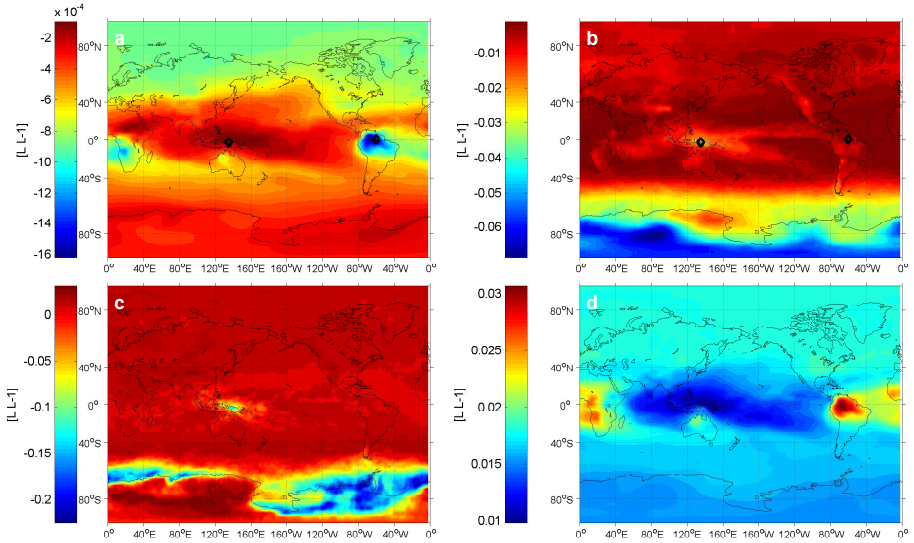

Figure 4. Annually-averaged accumulation mode dust number sensitivities for **(a)** PDA08, **(b)** PDA13, **(c)** CNT, and **(d)** AIDA.

ACPD
15, 21671–21711, 2015

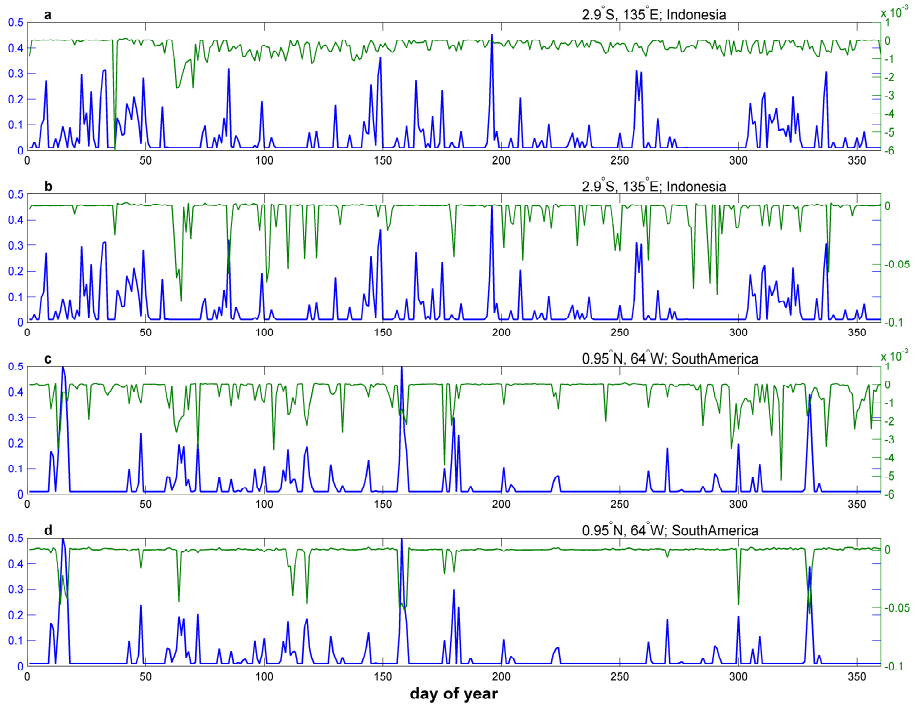

Figure 5. Time series of accumulation mode dust number sensitivities (green, in $\mathrm{L\,L^{-1}}$) and input updraft velocities (blue, in $\mathrm{m\,s^{-1}}$) over Indonesia at 2.9° S, 135° E for **(a)** PDA08 and **(b)** PDA13; and over South America at 0.95° N, 64° W for **(c)** PDA08 and **(d)** PDA13.

ACPD
15, 21671–21711, 2015

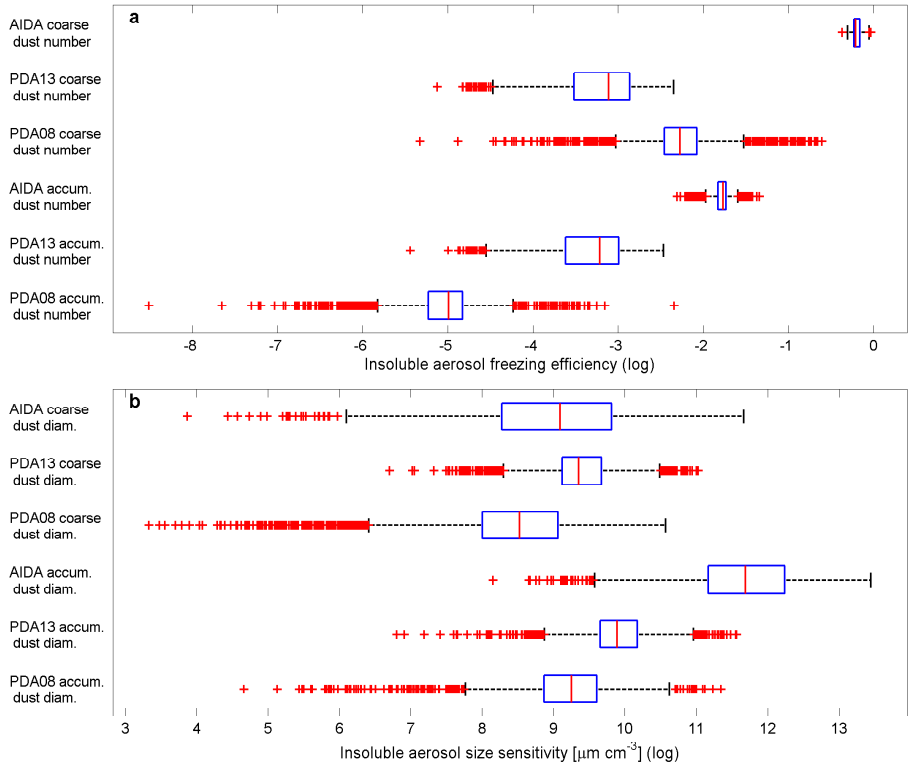

Figure 6. Log-space distributions of a random sampling of **(a)** accumulation and coarse mode dust number and **(b)** dust diameter for PDA08, PDA13, and AIDA spectra during purely heterogeneous nucleation. The box is constructed with 25th percentile, q_1; median, q_2; and 75th percentile, q_3. Outlying points are marked with crosses if they fall outside $[q_1 - 1.5(q_3 - q_1), q_3 + 1.5(q_3 - q_1)]$.

ACPD
15, 21671–21711, 2015